Proceedings of the Project Review, Geo-Mathematical Imaging Group (Purdue University, West Lafayette IN), Vol. 1 (2010) pp. 233-250.

A DISCONTINUOUS GALERKIN METHOD FOR MODELING MARINE CONTROLLED SOURCE ELECTROMAGNETIC DATA

TORGEIR WIIK*, MAARTEN V. DE HOOP†, AND BJØRN URSIN‡

Abstract. We give a brief introduction to the marine Controlled Source Electromagnetic method for hydrocarbon prospecting. A discontinuous Galerkin method is developed for the diffusive Maxwell's/MagnetoTelluric equations in this setting using linear finite element spaces. We utilize Perfectly Matched Layers based on a complex coordinate stretching, to emulate the radiation condition. Convergence tests on 1D diffusive Maxwell's equations are performed, which indicate a linear convergence. Further, the method seems to treat the medium discontinuities well, which is essential in mCSEM modeling due to the parameters varying over many orders of magnitude.

Keywords: Controlled source electromagnetic, discontinuous Galerkin, Maxwell's equations

1. Introduction. The use of low-frequency, electromagnetic signals in hydrocarbon prospecting is a relatively new achievement; the first Seabed Logging (SBL) survey was conducted by Statoil offshore Angola in 2000. Marine Controlled Source Electromagnetic (mCSEM) surveys are usually performed by towing a horizontal, electric dipole which outputs a square wave current, thus generating electromagnetic signals, behind a vessel. Usually the signal's frequencies lie in the range $0.1\text{Hz} - 10\text{Hz}$, as these frequencies penetrate into the relevant depths of the subsurface. Receivers that measure the electric and magnetic field are placed on the seabed (See Figure 1).

However, the idea of using electromagnetic signals for hydrocarbon prospecting is not new. The equipment used today was mostly developed at Scripps Institution of Oceanography [15], and experiments were carried out in 1979 [40, 50]. One of the first patents in this context was filed already in 1986 [41], but finding an appropriate configuration for hydrocarbon prospecting turned out to be difficult. Among the early works on this is [8, 7, 21]. For a more complete overview of the history, we refer to [14]. Indeed, the breakthrough did not occur until 2000 using the approach described in [19].

Much of the development since then has been presented in the 2007 March-April edition of Geophysics, which contained a special section devoted to mCSEM. This section discusses the history of mCSEM [14] and the basic physics [37, 11], as well as more complex 2D and 3D settings [26, 27, 22]. A Bayesian study integrating seismic data in the analysis was presented by [9]. Recently the development has moved towards complete modeling of the full 3D problem, primarily using finite differences [31, 44, 33]. In addition, a thorough study of propagation in 1D anisotropic media was performed in [30].

The method used by [19] uses the data in the frequency domain, as the square wave source signal yields an odd harmonic series of distinct frequencies. The theory concerning the time-domain counterpart can be found in e.g. [13, 39]. A wide band frequency domain survey should be similar to a time domain survey. However, Constable and Srnka [14] point to several operational reasons for why the frequency domain approach has been the method of choice for offshore hydrocarbon prospecting. The time domain response works well on land, as the less resistive subsurface (compared to air) implies that the subsurface information is contained in the late arrivals, while the opposite is true for marine acquisition due to the conductive water column. In the frequency domain however, the relatively resistive seabed rocks dictate that the subsurface information is contained at sufficiently large offsets, where the direct "wave" from source to receiver has been attenuated. The frequency domain approach also allows for focusing the energy at specific frequencies, allowing for a higher signal-to-noise ratio. Nevertheless, time domain methods have attracted interest also [51, 42]. We will focus on the frequency domain method.

*Department for Petroleum Engineering and Applied Geophysics, The Norwegian University of Science and Technology, S.P. Andersensvei 15A, 7491 Trondheim, Norway.

†Center for Computational and Applied Mathematics, Purdue University, 150 N. University Street, West Lafayette IN 47907, USA.

‡Department for Petroleum Engineering and Applied Geophysics, The Norwegian University of Science and Technology, S.P. Andersensvei 15A, 7491 Trondheim, Norway.

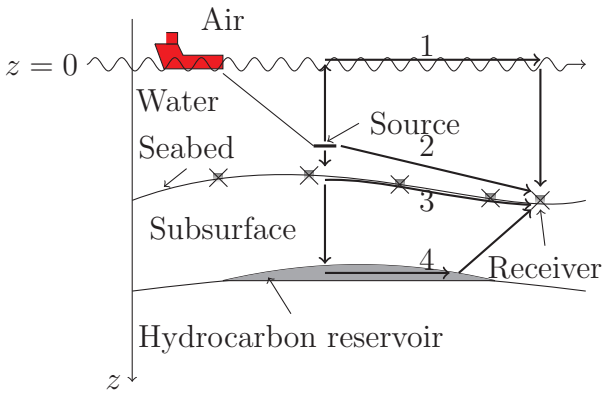

FIG. 1. *Figure displaying a usual configuration of a mCSEM survey. A horizontal electric dipole is towed behind a vessel, while receivers are placed on the seabed. Main sources for measured response are: 1:Reflection from sea-air interface, 2:direct wave, 3:Response from the seabed, 4:Response from hydrocarbon reservoir. The figure is retrieved from [29].*

The equations underlying the CSEM method are derived from the Maxwell equations, and coincide with the equations used for MagnetoTellurics (MT).

The electromagnetic properties of a medium are described by its electric permittivity, electric conductivity and magnetic permeability. A hydrocarbon reservoir will typically possess a lower electric conductivity compared to its surroundings, which means that the electromagnetic signals from the dipole will scatter when they hit the reservoir. From measuring this scattered field at the receivers we can be able to predict the location of a possible reservoir and what kind of fluid (oil, gas, water) it contains. Modeling this scattered response in known models constitutes the forward scattering problem, which we will consider in this paper.

However, recorded fields are not necessarily only the scattered field from an anomaly, which a hydrocarbon reservoir represents in the subsurface. As shown in Figure 1 there is response from several other factors, which may distort our results. At short source-receiver offsets, say less than 2km between source and receiver, the direct field from source to receiver dominates the recorded signals. At longer offsets the response from the seabed, the air wave and the scattered field from the hydrocarbon reservoir dominate, as the signal passes with a different decay through the hydrocarbon reservoir over longer distances due to the guided wave principle [48, 19, 25]; the low conductivity implies low attenuation. Despite using electromagnetic waves for hydrocarbon prospecting had been investigated, it was this idea of guided waves that allowed for the first successful application. The latter responses also contain multiple reflections in the water column and between layers in the subsurface, which imposes further problems in data processing, as the receivers will measure signals that are not only a consequence of primary events.

To model the response of a mCSEM experiment we apply the discontinuous Galerkin (DG) method, see [24] for an introduction. The DG method for elliptic problems originates from finite element methods using interior penalties (IP) to weakly enforce continuity conditions between elements, see for instance [2, 3, 18, 4, 49, 1]. The method is a mixture between conventional finite element methods and finite volume methods; over each element in the mesh the solution is expanded in a chosen basis, and to connect this element to its neighbors in a consistent way a numerical flux is specified along the element boundary. We use a formulation based on the first order system of equations, an approach which is similar to the method used by [17] and also closely related to the work in [20]. We note that the solution of Maxwell's equations using DG methods has also been studied in the context of second order *curl-curl* equations using IP methods, see for instance [38] and the references therein, and so called local DG methods [12, 6]. The first order system has advantages in as much as that one avoids numerical differentiation to obtain the "second" field,

as both the electric and magnetic field are observed in mCSEM. The motivation for applying the DG method to this problem lies in the treatment of discontinuities in the electromagnetic fields at material interfaces, i.e. geological interfaces, in the subsurface. Further, the DG method is flexible with respect to the computational mesh, which should prove an advantage for geophysical models. For instance, conventional finite difference and finite element methods usually require a very dense mesh around the source and material interfaces. This refinement can be expected to be relaxed using DG, as we allow a discontinuous representation of the solution.

We present a DG method for the mCSEM problem in $\mathbb{R}^3$ using linear basis functions to accomodate the limited regularity of the coefficients. The problem is formulated as a first order system, thus avoiding the penalty terms which are introduced in the IP *curl-curl* formulation. A Perfectly Matched Layer is implemented to simulate the radiation condition on the finite computational domain. This formulation using the DG method admits large jumps in the conductivity. This is essential for the mCSEM problem where the conductivity varies over many orders of magnitudes. We test the performance of our algorithm in 1D. The error of the scheme is estimated to decay linearily as a function of mesh size.

The purpose of this work is to provide a well defined setting for this problem and prove convergence of our algorithm to a unique solution. Further, computational physics experiments will be conducted in the context of inverse problems.

2. Basic equations.

2.1. Problem formulation. Let σ, ϵ and μ denote the electric conductivity, electric permittivity and magnetic permeability, which are assumed to be real, non-negative L^∞ functions. We further accept the constitutive relations $\mathbf{d} = \epsilon\mathbf{e}$, $\mathbf{b} = \mu\mathbf{h}$ and $\mathbf{j}^c = \sigma\mathbf{e}$, where $\mathbf{d}, \mathbf{e}, \mathbf{b}, \mathbf{h} \in \mathbb{C}^3$ are the electric displacement field, electric field, magnetic flux density and magnetic field strength, respectively, and $\mathbf{j}^c$ is the conduction current set up by an imposed electric field. This leads us to the following form of Maxwell's time harmonic curl equations in $\mathbb{R}^3$ [43]:

$$\nabla \times \mathbf{e} = \mathrm{i}\omega\mu_0\mathbf{h}, \tag{2.1}$$

$$\nabla \times \mathbf{h} = \tilde{\sigma}\mathbf{e} + \mathbf{j}^s, \tag{2.2}$$

where $\mathrm{i} = \sqrt{-1}$, $\omega = 2\pi f$, $\tilde{\sigma} = \sigma - \mathrm{i}\omega\epsilon$ and $\mathbf{j}^s$ is the source current density. Here f denotes the frequency and μ_0 is the freespace permeability.

The source $\mathbf{j}^s$ is a horizontal electric dipole for mCSEM applications, with polarization given by $l = [l_x, l_y, 0]^T$, where $|l|$ is the length of the source, and current amplitude $I(\omega)$. The source dipole moment is given by $I|l|$. This is well approximated by a point dipole, $Il\delta(\mathbf{x} - \mathbf{x}_s)$ when $|l| \ll \lambda$, where $\mathbf{x}_s$ is the source position and λ is the wavelength [29]. However, numerically we will use a normalized hat function, with increasing height as a function of decreasing width, as source. This implies that $\mathbf{j}^s \in \left[L^2\left(\mathbb{R}^3\right)\right]^3$ for a finite width, which is needed in the later weak formulation. The piecewise linear hat-shape is chosen as we will restrict ourselves to a linear basis. The source function is explicitly given later.

In our applications the frequencies lie in the range $0.1-10$Hz. In the watercolumn and sediments we have $\tilde{\sigma} \approx \sigma$, i.e. the quasi-static approximation [34] applies, which means that the equations describes a diffusion process instead of wave propagation. This is because of the low frequencies, the fact that the conductivity of sea-water is approximately 3.2S/m (around 1S/m for water filled sediments) and the permittivity is usually of the same order as the freespace permittivity, $\epsilon = \epsilon_0 = 8.85 \cdot 10^{-12}$F/m. These conditions allow us to neglect the displacement currents.

Further, we assume that the fields decay as they propagate towards infinity, which is expressed through the Silver-Müller radiation condition. This is expressed as [28]

$$\begin{cases} \left|\sqrt{\tilde{\epsilon}}\mathbf{e} - \mathbf{h} \times \frac{\mathbf{r}}{r}\right| \leq \frac{c}{r^2} \\ |\mathbf{e}| \leq \frac{c}{r} \\ |\mathbf{h}| \leq \frac{c}{r} \end{cases},$$

where $\tilde{\epsilon} = \epsilon + \mathrm{i}\frac{\sigma}{\omega}$, $\mathbf{r} = \mathbf{x}$, $r = |\mathbf{r}|$ and c is a generic constant.

We consider solving equations 2.1 and 2.2 on a bounded domain $\Omega \subset \mathbb{R}^3$ with appropriate boundary conditions imposed on $\partial\Omega$. These boundary conditions will be specified later, and will correspond to those introduced for the Perfectly Matched Layers (PML) as discussed in Appendix A. We introduce the Sobolev space

$$W = H(\mathrm{curl};\Omega) = \left\{ f \in \left[L^2(\Omega)\right]^3 : \nabla \times f \in \left[L^2(\Omega)\right]^3 \right\},$$

and assume $\mathbf{j}^s \in \left[L^2(\Omega)\right]^3$. We further denote for vectors $a, b \in \mathbb{C}^3$

$$(a,b)_\Omega = \int_\Omega a \cdot \bar{b} \mathrm{d}\mathbf{x},$$

where the overline denotes complex conjugate. We proceed by multiplying equations 2.1 and 2.2 with $v \in \mathcal{D}$, where $\mathcal{D}$ is a space of sufficiently smooth test functions, and integrating the result over Ω:

$$(\nabla \times \mathbf{e}, v)_\Omega = \mathrm{i}\omega\mu_0 (\mathbf{h}, v)_\Omega , \tag{2.3}$$

$$(\nabla \times \mathbf{h}, v)_\Omega = (\tilde{\sigma}\mathbf{e}, v)_\Omega + (\mathbf{j}^s, v)_\Omega . \tag{2.4}$$

Performing integration by parts then yields

$$\int_{\partial\Omega} \overline{v} \cdot (\mathbf{n} \times \mathbf{h}) \, \mathrm{d}S + (\mathbf{h}, \nabla \times v)_\Omega = (\tilde{\sigma}\mathbf{e}, v)_\Omega + (\mathbf{j}^s, v)_\Omega , \tag{2.5}$$

$$\int_{\partial\Omega} \overline{v} \cdot (\mathbf{n} \times \mathbf{e}) \, \mathrm{d}S + (\mathbf{e}, \nabla \times v)_\Omega = \mathrm{i}\omega\mu_0 (\mathbf{h}, v)_\Omega , \tag{2.6}$$

where $\mathbf{n}$ is the outward pointing unit normal and $\mathrm{d}S$ is a surface measure. This yields the following weak formulation of our problem:

Find $\mathbf{e}, \mathbf{h} \in W$ *such that equations 2.5 and 2.6 holds* $\forall v \in \mathcal{D}$.

The measurements $\mathbf{e}_{\mathrm{meas}}, \mathbf{h}_{\mathrm{meas}}$, taken along a line or on a surface $\mathcal{S}$, are then expressed as the restriction of $\mathbf{e}$ and $\mathbf{h}$ to $\mathcal{S}$. That is,

$$\mathbf{e}_{\mathrm{meas}} = \mathbf{e}(\mathbf{x}) \mid_{\mathcal{S}}, \mathbf{h}_{\mathrm{meas}} = \mathbf{h}(\mathbf{x}) \mid_{\mathcal{S}} .$$

2.2. Rays, asymptotic expansions. For later comparison with the results obtained using the DG method we present a short summary of the asymptotic ray expansion presented in [47, 16]. To this end we follow [16] and assume that the fields due an unit electric point source are asymptotically given by

$$\begin{cases} \mathbf{e}(\mathbf{x}) \sim e^{-\sqrt{-\mathrm{i}\omega}\tau(\mathbf{x})} \sum_{k=0}^{\infty} (-\mathrm{i}\omega)^{-(k-2)/2} e_k(\mathbf{x}) \\ \mathbf{h}(\mathbf{x}) \sim e^{-\sqrt{-\mathrm{i}\omega}\tau(\mathbf{x})} \sum_{k=0}^{\infty} (-\mathrm{i}\omega)^{-(k-1)/2} h_k(\mathbf{x}) \end{cases} ,$$

where $\tau(\mathbf{x})$ is the eikonal and e_k, h_k are the amplitudes. Inserting this into equations 2.1 and 2.2 in the quasi-static limit leads to the equivalents of the eikonal equation and transport equations of

the ray theory for the wave equation:

$$
\begin{aligned}
&\nabla\tau\cdot\nabla\tau=\sigma\mu_0,\\
&2\left(\nabla\tau\cdot\nabla\right)e_0+\left[\nabla\cdot\left(\nabla\tau\right)\right]e_0+\left(\frac{\nabla\sigma}{\sigma}\cdot e_0\right)\nabla\tau=0,\\
&2\left(\nabla\tau\cdot\nabla\right)h_0+\left[\sigma\nabla\cdot\left(\frac{1}{\sigma}\nabla\tau\right)\right]h_0+\left(\frac{\nabla\sigma}{\sigma}\cdot h_0\right)\nabla\tau=0,\\
&2\left(\nabla\tau\cdot\nabla\right)e_{m-1}+\left[\nabla\cdot\left(\nabla\tau\right)\right]e_{m-1}+\left(\frac{\nabla\sigma}{\sigma}\cdot e_{m-1}\right)\nabla\tau=\\
&\qquad\nabla\left[\frac{1}{\sigma}\nabla\cdot\left(\sigma e_{m-2}\right)\right]-\nabla\times\nabla\times e_{m-2},\quad m=2,3,4,\ldots,\\
&2\left(\nabla\tau\cdot\nabla\right)h_{m-1}+\left[\sigma\nabla\cdot\left(\frac{1}{\sigma}\nabla\tau\right)\right]h_{m-1}+\left(\frac{\nabla\sigma}{\sigma}\cdot h_{m-1}\right)\nabla\tau=\\
&\qquad\nabla\left[\nabla\cdot\left(h_{m-2}\right)\right]-\sigma\nabla\times\left(\frac{1}{\sigma}\nabla\times h_{m-2}\right),\quad m=2,3,4\ldots
\end{aligned}
\tag{2.7}
$$

It may be shown using the method of steepest descent to the field integrals that the asymptotic response from a thin resistive layer in an isotropic stratified model is due to a pole in the complex frequency plane of the reflection coefficient [29]. This should correspond to a guided rays in the resistor. The air-wave, i.e. the interaction at the sea/air interface, and other phenomena, may be accounted for in a similar way which also shown in [29]. The air-wave is an important phenomenon as it dominates the recorded signal at very far offsets, due to it passing with no attenuation through the air and leaking back towards the seabed. Due to the very high conductivity contrast at this interface it is also difficult to handle properly numerically, but the DG method should be able to handle this because of its inherent discontinuities.

3. Discontinuous Galerkin Method.

3.1. Mesh and approximation space. We solve equations 2.5 and 2.6 numerically for $\mathbf{e}$ and $\mathbf{h}$ using the DG method on a bounded domain $\Omega\subset\mathbb{R}^3$, where $\mathbf{n}\times\mathbf{e}=0$ is imposed on $\partial\Omega$. Inside $\partial\Omega$ a PML zone, where the fields are attenuated without causing any reflection back into the model, is incorporated to simulate the radiation condition, as shown in Figure 2. It is assumed that the air layer is chosen thick enough to account for the interaction between the water column and the air.

We consider $\Omega_h, h>0$, to be a family of discretized approximations to Ω such that $\overline{\Omega}_h=\bigcup_{K\in\tau_h}\overline{K}$, where τ_h is a tesselation of Ω_h into simplices, i.e. tetrahedrons in 3D. Figure 3 displays the intersection of a tetrahedral mesh with a local refinement embedded.

We denote the set of facets by Γ, facets between two neighboring elements by Γ^i and the facets on $\partial\Omega_h$ as Γ^b. Naturally $\Gamma=\Gamma^i\cup\Gamma^b$ and $\Gamma^i\cap\Gamma^b=\emptyset$.

We consider aproximative solutions $\left(\mathbf{e}^h,\mathbf{h}^h\right)\in X\times X$ which satisfy equations 2.5 and 2.6, where

$$
X=\left\{f\in\left[L^2\left(\Omega\right)\right]^3:\forall K\in\tau_h, f\mid_K\in\left[\mathcal{P}^1\left(K\right)\right]^3\right\}.
$$

Here $\mathcal{P}^1\left(K\right)$ is the space of polynomials of at most degree 1 over K. Since we consider a Galerkin type method, the space of test functions is chosen equal to the solution space.

It is easily verified that

$$
\begin{aligned}
&\Big\{\left[1,0,0\right]^T,\left[0,1,0\right]^T,\left[0,0,1\right]^T,\left[x',0,0\right]^T,\left[y',0,0\right]^T,\left[z',0,0\right]^T,\\
&\qquad\left[0,x',0\right]^T,\left[0,y',0\right]^T,\left[0,z',0\right]^T,\left[0,0,x'\right]^T,\left[0,0,y'\right]^T,\left[0,0,z'\right]^T\Big\}\\
&=\left\{v_K^i:i=1\ldots12\right\}=X_K
\end{aligned}
$$

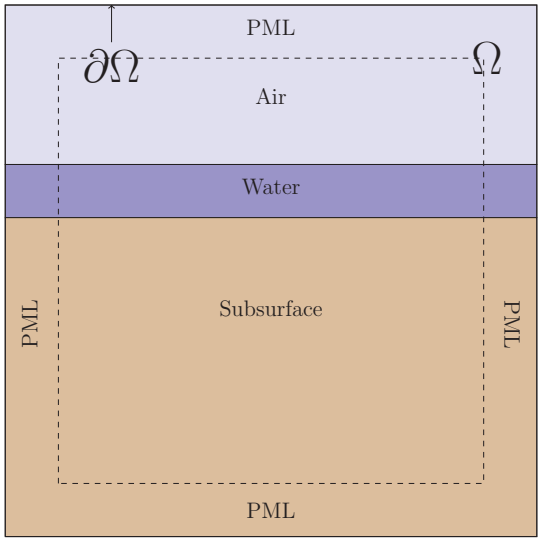

FIG. 2. *Intersection of domain* Ω.

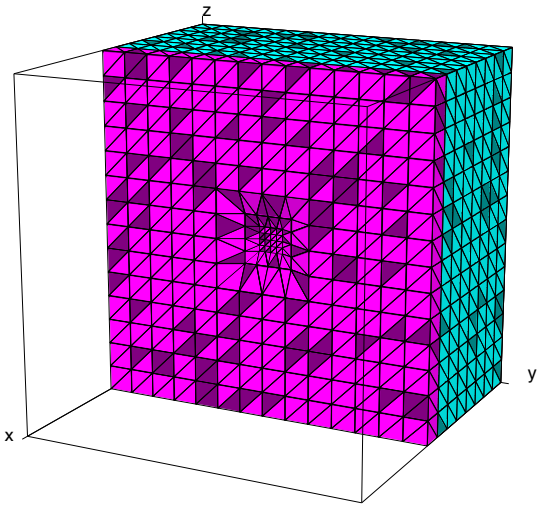

FIG. 3. *Example mesh.*

is a basis for X restricted to a given element K, where $x' = \frac{1}{L}(x - x_0)$, x_0 is a vertex of the tetrahedron and L is a characteristic lenght scale of the element. This choice is made to ensure that the expansion coefficients of the solutions in this basis have little dependency on the actual spatial positions of the elements, which should yield a better conditioned system to solve. This is called a modal basis, and differs from the nodal approach as described in [24] where basisfunctions are constructed around specific points within each element.

3.2. Local weak formulation. We obtain the local weak formulation for the discrete solution by considering the weak formulation over a single element $K \in \tau_h$:

$$\int_{\partial K} v \cdot (\mathbf{n} \times \mathbf{h}^*) \, \mathrm{d}S + \left(\mathbf{h}^h, \nabla \times v\right)_K = \left(\tilde{\sigma}\mathbf{e}^h, v\right)_K + \left(\mathbf{j}^s, v\right)_K , \tag{3.1}$$

$$\int_{\partial K} v \cdot (\mathbf{n} \times \mathbf{e}^*) \, \mathrm{d}S + \left(\mathbf{e}^h, \nabla \times v\right)_K = \mathrm{i}\omega\mu_0 \left(\mathbf{h}^h, v\right)_K , \tag{3.2}$$

where $\mathbf{e}^*, \mathbf{h}^*$ are the numerical fluxes which remain to be specified. This yields the following local discrete weak formulation of our problem:

Find $\mathbf{e}^h, \mathbf{h}^h \in X$ such that equations 3.2 and 3.1 hold $\forall v \in X$, for each $K \in \tau_h$.

To couple each element to its neighbours and to ensure consistency a numerical flux needs to be specified at the element boundaries, as the fields take on two values at each facet due to the discontinuities. Several choices for specifying the flux term have been explored, for instance the upwinding flux [17] is popular for flow problems. We choose to use the centered flux [17], as for the diffusion dominated problem there is no wave motion as such. We thus use

$$\mathbf{e}^* = \{\{\mathbf{e}\}\} = \frac{1}{2}\left(\mathbf{e}^{h,+} + \mathbf{e}^{h,-}\right),$$

and similarily for the magnetic field. Here $+/-$ denotes each side of the boundary surface. For element K we may write $\partial K = \bigcup_{k=1}^{4} F_k$, where F_k is a facet of the tetrahedron, and over each such facet the normal vector is constant. Since the pairwise intersection of facets on a given tetrahedron has zero surface measure we may write the integral as the sum of the integrals over each face. At the boundary $\partial\Omega_h$, where there are no neighbours, we implement the boundary condition $\mathbf{n} \times \mathbf{e} = 0$, and define $\mathbf{h}^* = \{\{\mathbf{h}\}\} = \mathbf{h}^{h,+}$, i.e. the limit of the value in the element. This may cause reflection at the boundary, but will nevertheless be attenuated by the PML zone.

3.3. Global weak formulation. The global weak formulation is obtained by summing equations 3.1 and 3.2 over the elements, thus obtaining

$$\sum_{F \in \Gamma^i} \int_F [[v]] \cdot (\mathbf{n} \times \{\{\mathbf{h}\}\}) \, \mathrm{d}S + \sum_{F \in \Gamma^b} \int_F v \cdot (\mathbf{n} \times \{\{\mathbf{h}\}\}) \, \mathrm{d}S + \sum_{K \in \tau_h} \left(\mathbf{h}^h, \nabla \times v\right)_K = \left(\tilde{\sigma}\mathbf{e}^h, v\right)_{\Omega_h} + \left(\mathbf{j}^s, v\right)_{\Omega_h} , \tag{3.3}$$

$$\sum_{F \in \Gamma^i} \int_F [[v]] \cdot (\mathbf{n} \times \{\{\mathbf{e}\}\}) \, \mathrm{d}S + \sum_{K \in \tau_h} \left(\mathbf{e}^h, \nabla \times v\right)_K = \mathrm{i}\omega\mu_0 \left(\mathbf{h}^h, v\right)_{\Omega_h} , \tag{3.4}$$

where $[[v]] = I_{FK} v + I_{F\tilde{K}} v$, $I_{FK} = \pm 1$ depending on the orientation of the normal vector $\mathbf{n}$ chosen for that facet and $\tilde{K}$ is a neighbor of K. This means that $[[v]]$ is the *jump* of v. This yields the following global discrete weak formulation of our problem:

Find $\mathbf{e}^h, \mathbf{h}^h \in X$ such that equations 3.4 and 3.3 holds $\forall v \in X$.

3.4. Boundary and interface operators. At this point it is straightforward to make the connection to the boundary operator M_F for $F \in \Gamma^b$ and the interface operator D_F for $F \in \Gamma^i \cup \Gamma^b$

as presented in [20]. To do this we first separate the source term and write

$$\left(\tilde{\sigma}\mathbf{e}^h, v\right)_{\Omega_h} - \sum_{F\in\Gamma^i}\int_F [[v]]\cdot(\mathbf{n}\times\{\{\mathbf{h}\}\})\,\mathrm{d}S - \sum_{F\in\Gamma^b}\int_F v\cdot(\mathbf{n}\times\{\{\mathbf{h}\}\})\,\mathrm{d}S -$$

$$\sum_{K\in\tau_h}\left(\mathbf{h}^h, \nabla\times v\right)_K = -\left(\mathbf{j}^s, v\right)_{\Omega_h}, \tag{3.5}$$

$$\mathrm{i}\omega\mu_0\left(\mathbf{h}^h, v\right)_{\Omega_h} - \sum_{F\in\Gamma^i}\int_F [[v]]\cdot(\mathbf{n}\times\{\{\mathbf{e}\}\})\,\mathrm{d}S - \sum_{K\in\tau_h}\left(\mathbf{e}^h, \nabla\times v\right)_K = 0. \tag{3.6}$$

We rewrite this as a single equation for $\mathbf{w}^h = \left(\mathbf{e}^h, \mathbf{h}^h\right) \in X\times X$ as

$$\int_{\Omega_h} G_0\mathbf{w}^h\cdot\tilde{v}\mathrm{d}\mathbf{x} - \sum_{F\in\Gamma^i}\int_F [[\tilde{v}]]\cdot G_{\mathbf{n}}\{\{\mathbf{w}\}\}\,\mathrm{d}S - \sum_{F\in\Gamma^b}\int_F \tilde{v}\cdot G_{\mathbf{n}}\{\{\mathbf{w}\}\}\,\mathrm{d}S -$$

$$\sum_{K\in\tau_h}\int_K \mathbf{w}^h\cdot\sum_{l=x,y,z} G_{\mathbf{e}_l}\frac{\partial}{\partial l}\tilde{v}\mathrm{d}\mathbf{x} = -\int_{\Omega_h}\mathbf{j}\cdot\tilde{v}\mathrm{d}\mathbf{x}, \tag{3.7}$$

where $\tilde{v}\in X\times X$ and $\mathbf{j} = [\mathbf{j}^s, 0_{1\times 3}]^T$, and

$$G_0 = \begin{pmatrix} \tilde{\sigma}I_{3\times 3} & 0_{3\times 3} \\ 0_{3\times 3} & \mathrm{i}\omega\mu_0 I_{3\times 3}\end{pmatrix}, G_{\mathbf{n}} = \begin{pmatrix} 0 & N \\ N & 0\end{pmatrix}, N = \begin{pmatrix} 0 & -n_z & n_y \\ n_z & 0 & -n_x \\ -n_y & n_x & 0\end{pmatrix};$$

$\mathbf{e}_l$ is the canonical basis for $\mathbb{R}^3$. Following [20] we assume that M_F and D_F are associated with matrix valued fields, $\mathcal{M}_F : \Gamma^b \to \mathbb{R}^{6,6}$ and $\mathcal{D}_F : \Gamma^b\cup\Gamma^i \to \mathbb{R}^{6,6}$, respectively. We find that

$$\mathcal{D}_F = -G_{\mathbf{n}}, \tag{3.8}$$

$$\mathcal{M}_F = -\tilde{G}_{\mathbf{n}}, \tag{3.9}$$

with

$$\tilde{G}_{\mathbf{n}} = \begin{pmatrix} 0 & N \\ -N & 0\end{pmatrix}.$$

This specifies the actions of the operators on a vector through the matrix-vector product. It is evident that multiplication with N corresponds to the cross product with $\mathbf{n}$, and the construction of $G_{\mathbf{n}}, \tilde{G}_{\mathbf{n}}$ ensures that $\mathbf{n}\times\mathbf{e}$ vanishes on the boundary.

It may be verified that our system does not fit into the Friedrichs's systems framework treated by [20] because of the fact that the coefficients are complex, nor does the central flux satisfy the conditions set in [20] on boundary and interface operators for convergence. We note that on $F\in\Gamma^i$, $\mathcal{D}_F$ is double valued, although its mean is zero, while on Γ^b, $\mathcal{D}_F$ is single valued.

4. Discrete system. Over a given element K we write $\mathbf{e}^h\mid_K = a^0_{e,K}v^0_K + \ldots + a^{12}_{e,K}v^{12}_K$ and $\mathbf{h}^h\mid_K = a^0_{h,K}v^0_K + \ldots + a^{12}_{h,K}v^{12}_K$, where $v^i_K \in X_K$ and $a^i_{e/h,K}\in\mathbb{C}, i = 1\ldots 12$. We insert these representations into equations 3.3 and 3.4, which yields 24 equations to determine the 24 unknown expansion coefficients over K, coupled to the expansion coefficients of the neighbouring elements through the flux.

We note that each integral in the weak formulation can be calculated analytically, with the exception of $\left(\tilde{\sigma}\mathbf{e}^h, v\right)_K$ since $\tilde{\sigma}$ is allowed to vary within K, and perhaps the source integral depending on the source. These integrals are evaluated using Gaussian quadrature.

To this end we introduce $\phi_{i;j}$ such that $X = span\{\phi_{i;j} : i = 1\ldots 12, j = 1\ldots N_K\}$, where N_K is the number of elements. Specifically, we choose for a given $j = j_0$,

$$\phi_{i;j_0}(\mathbf{x}) = \begin{cases} v^i_{K_{j_0}}(\mathbf{x}), & \mathbf{x}\in K_{j_0} \\ 0, & elsewhise\end{cases},$$

where we have introduced an ordering of the elements. We may organize the system of equations as

$$\begin{pmatrix} A & B \\ B & C \end{pmatrix} \begin{pmatrix} E \\ H \end{pmatrix} = \begin{pmatrix} J \\ 0_{12N_K \times 1} \end{pmatrix},$$

where $A, B, C \in \mathbb{C}^{12N_K \times 12N_K}$, $E, H \in \mathbb{C}^{12N_K}$ contains the unknown expansion coefficients, and $J \in \mathbb{C}^{12N_K}$ contains the terms from the source integral. Specifically,

$$E = \left[a^1_{e,K_1}, \ldots, a^{12}_{e,K_1}, a^1_{e,K_2}, \ldots, a^{12}_{e,K_{N_K}} \right]^T,$$
$$H = \left[a^1_{h,K_1}, \ldots, a^{12}_{h,K_1}, a^1_{h,K_2}, \ldots, a^{12}_{h,K_{N_K}} \right]^T.$$

Disregarding the boundary conditions, which are implemented in the PML-zone, we find for $i, j = 1 \ldots N_K$ that the matrices are given by the following sub-matrices:

$$(A)_{ij} = \begin{pmatrix} (\tilde{\sigma}\phi_{1;i}, \phi_{1;j})_{K_i} & \cdots & (\tilde{\sigma}\phi_{1;i}, \phi_{12;j})_{K_i} \\ \vdots & \ddots & \vdots \\ (\tilde{\sigma}\phi_{12;i}, \phi_{1;j})_{K_i} & \cdots & (\tilde{\sigma}\phi_{12;i}, \phi_{12;j})_{K_i} \end{pmatrix},$$
$$-(B)_{ij} = \begin{pmatrix} \frac{1}{2} I^{\partial K_i}_{i,j,1,1} + \delta_{ij} I^{K_i}_{i,j,1,1} & \cdots & \frac{1}{2} I^{\partial K_i}_{i,j,1,12} + \delta_{ij} I^{K_i}_{i,j,1,12} \\ \vdots & \ddots & \vdots \\ \frac{1}{2} I^{\partial K_i}_{i,j,12,1} + \delta_{ij} I^{K_i}_{i,j,12,1} & \cdots & \frac{1}{2} I^{\partial K_i}_{i,j,12,12} + \delta_{ij} I^{K_i}_{i,j,12,12} \end{pmatrix},$$
$$(C)_{ij} = \mathrm{i}\omega\mu_0 \begin{pmatrix} (\phi_{1;i}, \phi_{1;j})_{K_i} & \cdots & (\phi_{1;i}, \phi_{12;j})_{K_i} \\ \vdots & \ddots & \vdots \\ (\phi_{12;i}, \phi_{1;j})_{K_i} & \cdots & (\phi_{12;i}, \phi_{12;j})_{K_i} \end{pmatrix},$$

where

$$I^{\partial K_i}_{i,j,k,l} = \int_{\partial K_i} \phi_{k;i} \cdot (\mathbf{n}_{K_i} \times \phi_{l;j}) \, \mathrm{d}S,$$
$$I^{K_i}_{i,j,k,l} = (\nabla \times \phi_{k;i}, \phi_{l;j})_{K_i},$$

$\mathbf{n}_{K_i}$ is the outward unit normal vector for element K_i and δ_{ij} is Krönecker's delta. We observe that with the given choice of basis for X both A and C are block diagonal, while B is a sparse matrix with entries along the diagonal and positions corresponding to neighbours. For the source term we find that

$$J = -\left[(\phi_{1;1}, \mathbf{j}^s)_{K_1}, \ldots, (\phi_{1;11}, \mathbf{j}^s)_{K_1}, (\phi_{1;2}, \mathbf{j}^s)_{K_2}, \ldots, (\phi_{11;N_K}, \mathbf{j}^s)_{K_{N_K}} \right]^T.$$

An example of the matrix structure for a small domain is shown in Figure 4. Every point corresponds to a block of either A, B or C. The blue points are the blocks on the diagonal of each submatrix, while the red are off-diagonal. The cloud-like pattern in the off-diagonal submatrices is due to the unstructured tetrahedral mesh, and suggests that the system is very poorly conditioned in this form. Finding an appropriate preconditioner is thus essential, and is discussed further in a later section.

4.1. Gaussian quadrature. A quadrature rule is an approximation to a definite integral of a function stated as a weighted sum of the function values chosen at specific points within the domain of integration. A n-point Gaussian quadrature rule is constructed to yield the exact result for polynomials of degree $2n - 1$ by suitably choosing the evaluation points x_i and weights w_i for

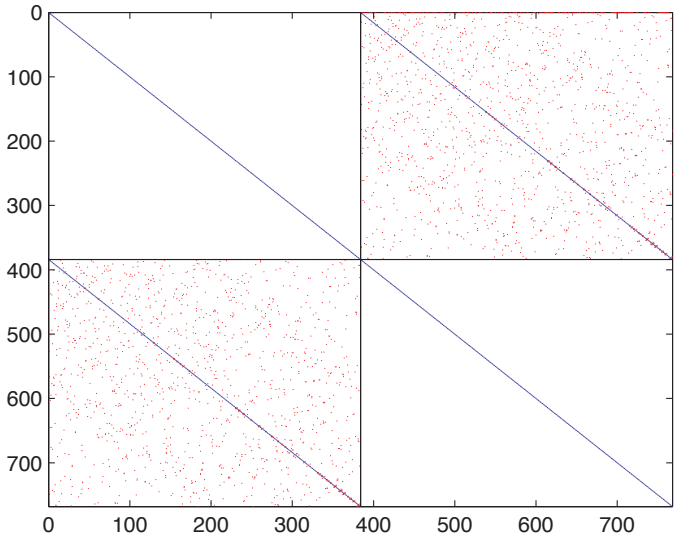

FIG. 4. *Matrix structure for a small domain.*

$i = 1 \dots n$. For the one-dimensional integral the standard case is usually expressed on the interval $[-1, 1]$ as

$$\int_{-1}^{1} f(x)\,\mathrm{d}x \approx \sum_{i=1}^{n} w_i f(x_i).$$

It can be shown that the evaluation points should be choosen as the roots of a class of polynomials.

To extend this to the tetrahedral case, n^3 points are arranged in a distorted cube inside the tetrahedron with the appropriate weights. See [45] for a more detailed description on quadrature rules in general and for the tetrahedron.

4.2. 3D Source representation. Due to the restriction to a linear basis we choose to implement the source as a L^2 normalized cone over $\mathbb{R}^3$ as

$$\mathbf{j}^s = \begin{cases} \frac{3}{\pi\tau^4}(\tau - r)\,\hat{\mathbf{d}}, & r \leq \tau \\ 0, & elsewhise \end{cases},$$

where $r^2 = (x - x_s)^2 + (y - y_s)^2 + (z - z_s)^2$ is the squared euclidian distance to the source and $\hat{\mathbf{d}} = [\cos\alpha, \sin\alpha, 0]^T$ describes the source polarization, where α is the angle between the source polarization and the x-axis in the horizontal plane. This choice is made as we model a horizontal electric dipole. Although its support is spherical the source's value increases linearly, which should be well approximated by the linear basis. An illustration of the 1D equivalent is shown in Figure 5.

4.3. Preconditioning. As mentioned previously, the discrete system of equations can often be quite stiff. This is especially true when the parameters vary over many orders of magnitude from air to sea water. We thus apply a preconditioner to the system. Two options are compared on the 1D example considered in the next section, a Jacobi preconditioner and an incomplete LU factorization. We find that both approaches reduce the condtition number of the system matrix, but the LU factorization is superior in this case, clustering the eigenvalues around the line $\Re(\lambda) = 1$ with $\Im(\lambda) \leq 1$, as shown in Figure 6. The incomplete LU factorization was perfomed with a cutoff at 10^{-3}.

FIG. 5. *1D hat source.*

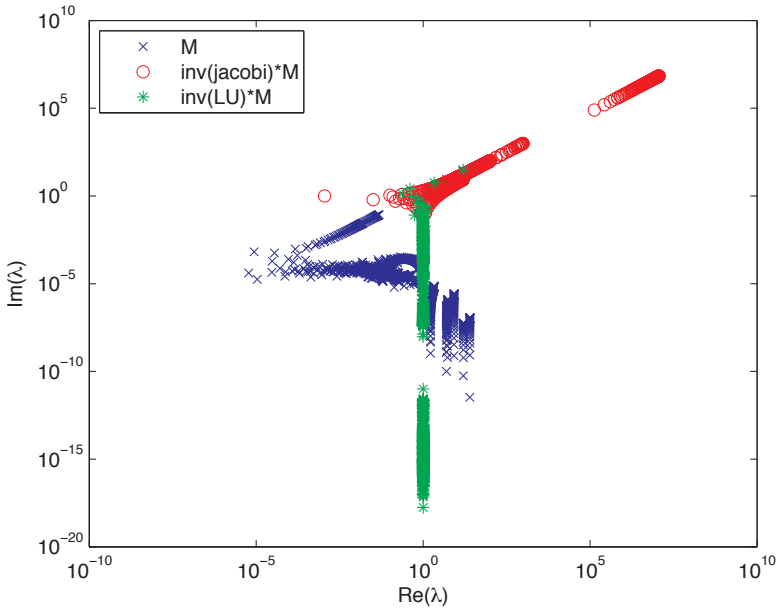

FIG. 6. *Eigenvalues of system matrix under different preconditioners. Blue cross: no preconditioner, red circle: Jacobi preconditioner, green star: incomplete LU preconditioner.*

5. Numerical experiments in 1D. As a demonstration of concept we consider the 1D Maxwell's equations; we restrict the propagation to the x-direction, assume that the medium parameters depend only on this coordinate and align the coordinate system such that $\mathbf{e} = [0, 0, e_z]^T$, $\mathbf{h} = [0, h_y, 0]^T$. This yields

$$\tilde{\sigma} e_z - \frac{\partial h_y}{\partial x} = -j^s,$$
$$\mathrm{i}\omega\mu_0 h_y + \frac{\partial e_z}{\partial x} = 0.$$

The source is chosen as a hat function with width κ given by

$$j^s(x) = \begin{cases} \frac{1}{\kappa^2}(x - x_s) + \frac{1}{\kappa}, & x_s - \kappa \leq x \leq x_s \\ -\frac{1}{\kappa^2}(x - x_s) + \frac{1}{\kappa}, & 0 \leq x \leq x_s + \kappa \\ 0, & elsewhere \end{cases},$$

which is normalized with respect to the $L^2(\Omega)$ norm. Here x_s is the center of the source which is set to $x = 350$m, and we consider the typical mCSEM frequency 0.25Hz. Due to the relatively low computational cost associated with 1D problems we have chosen to use uniform mesh sizes h. The results presented uses 350 intervals, which corresponds to $h = 10$m, including 500m PML zone in each end, and $\kappa = 10$m. Figure 7 displays the profile of the model which is considered.

Figure 8 displays estimated $L^2(\Omega)$ error of the magnetic field against a "truth" solution using 1400 elements. We observe that the convergence appears to be approximately linear in h, especially when the mesh size h approaches 10m, which is needed to resolve the source properly. The same is observed for the electric field. This is in compliance with the theoretical bounds referred to in the

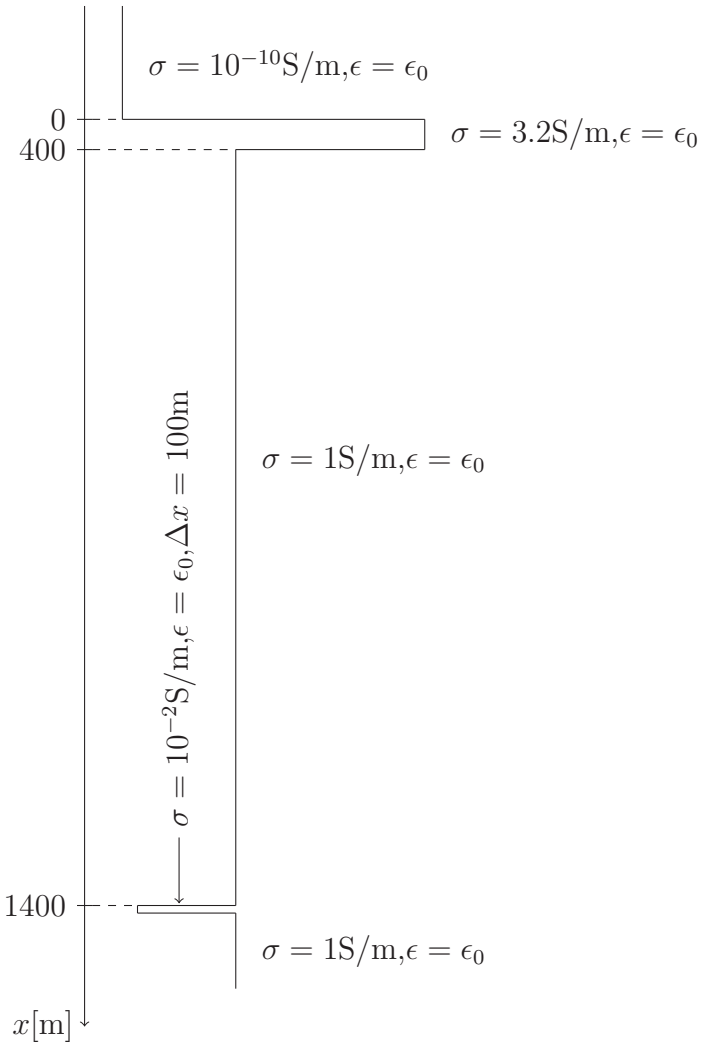

FIG. 7. *Model used in numerical example.*

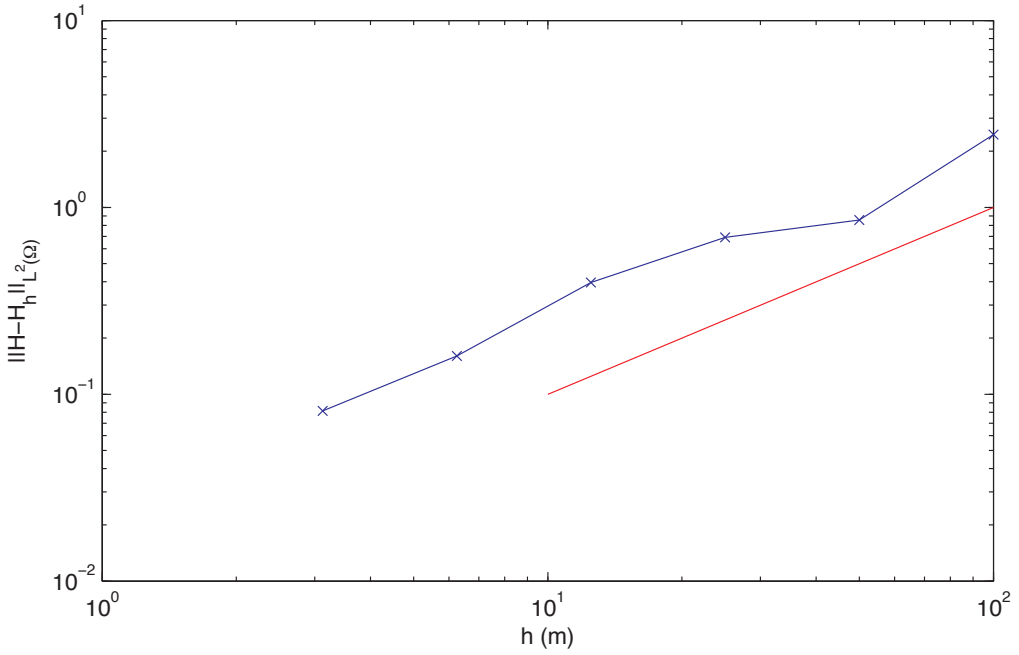

FIG. 8. *Convergence plot for magnetic field. Red line:* h^1.

investigations made by [17], but not in compliance with the quadratic convergence they report for the magnetic field in their numerical examples.

Figures 9(a) and 9(b) display the magnitude of the calculated magnetic field over the whole model and zoomed in around the source location, respectively. Figure 9(b) shows how well the DG method performs around the difficult source point and the interface at $x = 400$m, which should make it appropriate for mCSEM modeling.

6. Discussion. Preliminary tests applying the DG method to the 1D Maxwell equations show promise for applying this method to mCSEM modeling. The method is flexible with respect to the mesh construction and is able to handle large contrasts in properties at material interfaces due to its discontinuous nature. The accuracy of the method is estimated to increase linearily as a function of the mesh size. However, the corresponding linear system of equations is often very stiff due to the unstructured nature of tetrahedral meshes in 3D. Thus, finding an appropriate preconditioner is essential. Tests on a 1D problem suggest that an incomplete LU-type factorization is a good choice.

The DG implementation can be naturally tied to Automatic Differentiation [35, 23] for the purpose of sensitivity analysis and parameter analysis via Output Least Squares [46, 32].

7. Acknowledgements. The authors would like to acknowledge the help from Assistant Professor Peijun Li of Purdue University with the PML formulation. Torgeir Wiik acknowledges Statoil ASA for sponsoring his Ph.D. project. Bjørn Ursin has received financial support from VISTA and from the Norwegian Research Council through the ROSE project. The research was supported in part by the members of GMIG at Purdue University

Appendix A. PML boundaries. To simulate the radiation condition given in equation 2.1 with equations 2.1 and 2.2 one would need a huge domain Ω. This again would increase the computational cost significantly due to the large model. To avoid this, a strategy using *Perfectly Matched Layers* (PML) was invented. This involves padding the domain Ω with an absorbing medium to ensure that the fields are attenuated fast when they approach $\partial\Omega$, as indicated in Figure

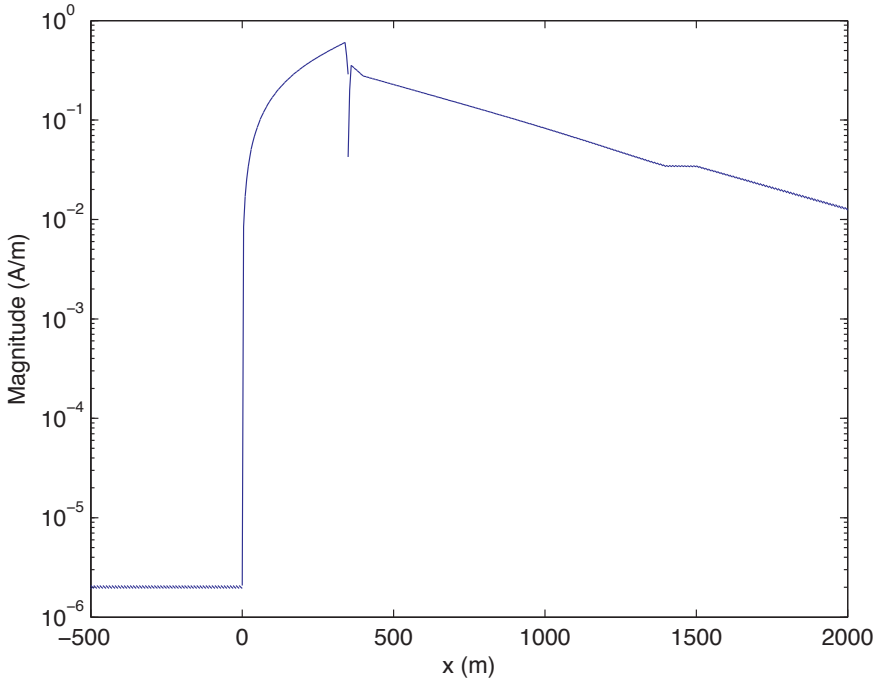

(a) Magnitude of h_y.

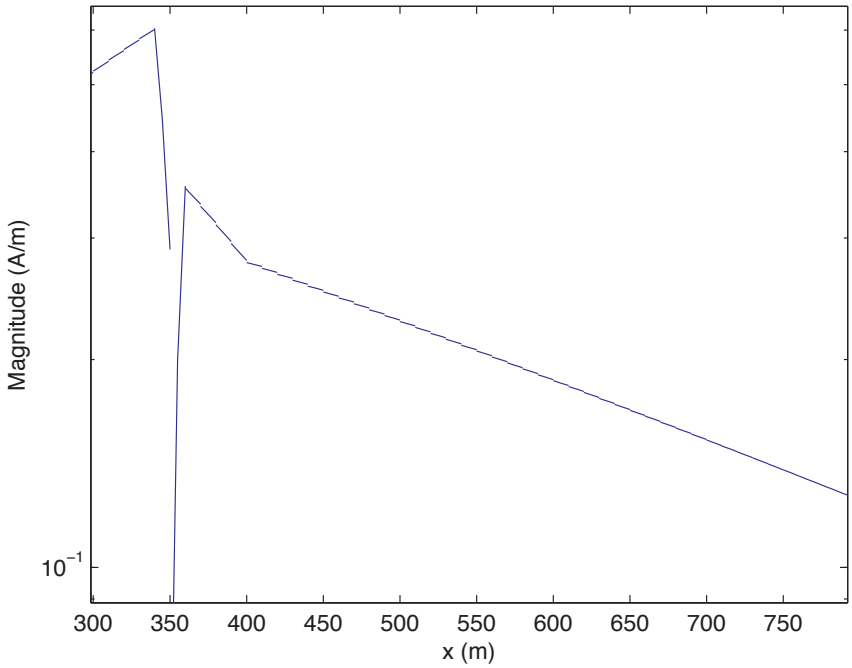

(b) Magnitude of h_y, zoomed in on source region.

FIG. 9. *Magnitude of magnetic field as a function of depth.*

2. However, the introduction of such a layer is not trivial. If it is done carelessly reflections from the boundary between the normal domain and the PML will be encountered, and these will potentially pollute the solution. To avoid these reflections from the boundary the PML is designed in such a way that the fields are attenuated within this zone, but it has no contrast in impedances compared to the actual domain of interest and thus does not cause any reflections. This attentuation emulates the radiation condition, and allows for a significantly smaller computational domain to be chosen. Several approaches are possible, for instance the variable splitting presented by Berenger [5] and anisotropic matching [36], but we choose the complex coordinate stretching, also known as complex scaling in analysis, introduced in [10].

To this end we follow [10] and introduce the complex coordinates

$$\begin{aligned} \tilde{x} &= \int_0^x s_x\left(x'\right) \mathrm{d}x', \\ \tilde{y} &= \int_0^y s_y\left(y'\right) \mathrm{d}y', \\ \tilde{z} &= \int_0^z s_z\left(z'\right) \mathrm{d}z', \end{aligned} \tag{A.1}$$

where $s_j(\tau) = \zeta_j^1(\tau) + \mathrm{i}\zeta_j^2(\tau)$ is a continuous function satisfying

$$\begin{aligned} \zeta_j^1 &= 1, \quad \zeta_j^2 = 0 \quad \text{outside the PML zone,} \\ \zeta_j^1 &\geq 1, \quad \zeta_j^2 > 0 \quad \text{inside the PML zone,} \end{aligned}$$

such that the coordinates coincides with the ordinary cartesian coordinates outside the PML zone. The gradient in the stretched coordinate system becomes

$$\tilde{\nabla} = \left[\frac{\partial}{\partial \tilde{x}}, \frac{\partial}{\partial \tilde{y}}, \frac{\partial}{\partial \tilde{z}}\right],$$

where $\frac{\partial}{\partial \tilde{x}} = \frac{1}{s_x}\frac{\partial}{\partial x}$. Maxwell's equations then become

$$\tilde{\nabla} \times \mathbf{e} = \mathrm{i}\omega\mu_0\mathbf{h}, \tag{A.2}$$

$$\tilde{\nabla} \times \mathbf{h} = \tilde{\sigma}\mathbf{e} + \mathbf{j}^s, \tag{A.3}$$

$$\tilde{\nabla} \cdot (\epsilon\mathbf{e}) = 0, \tag{A.4}$$

$$\tilde{\nabla} \cdot (\mu_0\mathbf{h}) = 0, \tag{A.5}$$

which looks as usual, except the coordinates may be complex. In practice $s_j(\tau)$ is taken as a power function, that is

$$s_j(\tau) = 1 + \chi\left(\frac{d(\tau)}{\delta}\right)^m, \quad m \geq 1,$$

where $d(\tau)$ is the distance in the j-direction to the boundary between the ordinary zone and the PML zone and δ is the thickness of the PML zone. It can be verified that increasing the thickness δ or increasing $\mathrm{Re}(\chi)$ and $\mathrm{Im}(\chi)$ will reduce the PML approximation error.

Appendix B.

[1] D Arnold. An interior penalty finite-element method with discontinuous elements. *SIAM Journal on Numerical Analysis*, 19:742–760, 1982.

[2] I Babuška. The finite element method with penalty. *Math. Comp.*, 27:221–228, 1973.

[3] I Babuška and M Zlámal. Nonconforming elements in th finite element method with penalty. *SIAM Journal on Numerical Analysis*, 10:863–875, 1973.

[4] G Baker. Finite element methods for elliptic equations using non-conforming elements. *Math. Comp.*, 31:45–59, 1977.
[5] J Berenger. Three-dimensional perfectly matched layer for the absorption of eletromagnetic waves. *Journal of Computational Physics*, 127:363–379, 1996.
[6] A L Buffa and I Perugia. Discontinuous galerkin approximation of the maxwell eigenproblem. *SIAM Journal on Numerical Analysis*, 44:2198–2226, 2006.
[7] A D Chave, S Constable, and R N Edwards. *Electromagnetic methods in Applied Geophysics*, volume 2: Application, chapter Electrical exploration methods for the seafloor, pages 931–966. Society of Exploration Geophysicists, Oklahoma, 1991.
[8] A D Chave and C S Cox. Controlled electromagntic sources for measuring electrical conductivity beneath the oceans. *Journal of Geophysical Research*, 87:5327–5338, 1982.
[9] J Chen, D Hoversten G M, Vasco, Y Rubin, and Z Hou. A bayesian model for gas saturation estimation using marine seismic ava and csem data. *Geophysics*, 72:WA85–WA95, 2007.
[10] W C Chew, J M Jin, and E Michielssen. Complex coordinate stretching as a generalized absorbing boundary condition. *Microwave and Optical Tehnology Letters*, 15:363–369, 1997.
[11] N B Christensen and K Dodds. 1d inversion and resolution analysis of marine csem data. *Geophysics*, 72:WA27–WA38, 2007.
[12] B Cockburn and C Shu. The local discontinuous galerkin method for time-dependent convection-diffusion systems. *SIAM Journal on Numerical Analysis*, 35:2440–2463, 1998.
[13] L Combee. *Transient diffusive electromagnetic fields in layered anisotropic media*. PhD thesis, TU Delft, 1991.
[14] S Constable and L J Srnka. An introduction to marine controlled-source electromagnetic methods for hydrocarbon exploration. *Geophysics*, 72:WA3–WA12, 2007.
[15] C S Cox. On the electrical conductivity of the oceanic lithosphere. *Physics of the Earth and Planetary Interiors*, 25:196–201, 1981.
[16] A T de Hoop, M L Oristaglio, T M Habashy, and C Torres-Verdin. Asymptotic ray theory for transient diffusive electromagnetic fields. *Radio Science*, 31:41–49, 1996.
[17] V Dolean, H Fol, S Lanteri, and R Perrussel. Solutionof the time-harmonic maxwell equations using discontinuous galerkin methods. *Journal of Computational and Applied Mathematics*, 218:435–445, 2008.
[18] J Douglas Jr and T Dupont. Interior penalty procedures for elliptic and parabolic galerkin methods. In *Lecture notes in physics*. Springer, Berlin, 1976.
[19] T Eidesmo, S Ellingsrud, L M MacGregor, S Constable, M C Sinha, S Johansen, F N Kong, and H Westerdal. Sea bed logging (sbl), a new method for remote and direct identification of hydrocarbon filled layers in deepwater areas. *First Break*, 20:144–152, 2002.
[20] A Ern and J-L Guermond. Discontinuous galerkin methods for friedrichs' systems. part i. general theory. *SIAM Journal on Numerical Analysis*, 44:753–778, 2006.
[21] A H Flosadóttir and S Constable. Marine controlled-source electromagnetic sounding. 1. modeling and experimental design. *Journal of Geophysical Research*, 101:5507–5517, 1996.
[22] A Gribenko and Zhdanov M. Rigorous 3d inversion of marine csem data based on the integral equation method. *Geophysics*, 72:WA73–WA84, 2007.
[23] A Griewank. *Evaluating Derivatives: Principles and Techniques of Algorithmic Differentiation*. SIAM, 2000.
[24] J S Hesthaven and T Warburton. *Nodal Discontinuous Galerkin Methods. Algorithms, Analysis, and Applications.* Springer New York, 2008.
[25] F N Kong, H Westerdal, S Ellingsrud, T Eidesmo, and S E Johansen. Seabed logging: a possible direct hydrocarbon indicator for deepsea prospects using EM energy. *Oil & Gas journal*, May 13, 2002.
[26] Y Li and K Key. 2d marine controlled-source electromagnetic modeling: Part 1 an adaptive finite-element algorithm. *Geophysics*, 72:WA51–WA62, 2007.
[27] Y Li and K Key. 2d marine controlled-source electromagnetic modeling: Part 2 the effect of bathymetry. *Geophysics*, 72:WA63–WA71, 2007.

[28] Y Liu, Q Hu, and D Yu. A non-overlapping domain decomposition for low-frequency time-harmonic maxwells equations in unbounded domains. *Advances in Computational Mathematics*, 28:355–382, 2008.
[29] L O Løseth. *Modelling of controlled source electromagnetic data*. PhD thesis, Norwegian University of Science and technology, 2007.
[30] L O Løseth and B Ursin. Electromagnetic fields in planarly layered anisotropic media. *Geophysical Journal International*, 170:44–80, 2007.
[31] F A Maaø. Fast finite-difference time-domain modeling for marine-subsurface electromagnetic problems. *Geophysics*, 72:A19–A23, 2007.
[32] S E Minkoff and W W Symes. Full waveform inversion of marine reflection data in the plane-wave domain. *Geophysics*, 62:540–553, 1997.
[33] R Mittet. High-order finite-difference simulations of marine csem surveys using a correspondence principle for wave and diffusion fields. *Geophysics*, 75:F33, 2010.
[34] M N Nabighian, editor. *Electromagnetic Methods in Applied Geophysics*. SEG, 1987.
[35] L B Rall. *Automatic Differentiation: Techniques and Applications*. Springer, 1981.
[36] Z S Sacks, D M Kingsland, R Lee, and J Lee. A perfectly matched anisotropic absorber for use as an absorbing boundary condition. *IEEE Transactions on Antennas and Propagation*, 43:1460–1463, 1995.
[37] E Schankee Um and D L Alumbaugh. On the physics of the marine controlled-source electromagnetic method. *Geophysics*, 72:WA13–WA26, 2007.
[38] A Schneebeli. *Interior Penalty Discontinuous Galerkin Methods for Electromagnetic And Acoustic Wave Equations*. PhD thesis, Universität Basel, 2006.
[39] E c Slob. *Scattering of transient diffusive electromagnetic fields*. PhD thesis, TU DElft, 1994.
[40] F N Spiess, K C Macdonald, T Atwater, R Ballard, A Carranza, D Cordoba, C Cox, V M Diaz Garcia, J Francheteau, J Guerrero, J Hawkings, R Haymon, R Hessler, T Juteau, M Kastner, R Larson, B Luyendyk, J D Macdougall, S Miller, W Normark, J Orcutt, and C Rangin. East pacific rise: Hot springs and geophysical experiments. *Science*, 207:1421–1433, 1980.
[41] L J Srnka. Method and apparatus for offshore electromagnetic sounding utilizing wavelength effects to determine optimum source and detector positions, 1986.
[42] K M Strack, N Allegar, and S Ellingsrud. Marine time domain csem: an emerging technology. In *SEG Las Vegas 2008 Annual Meeting, Expanded Abstracts*, 2008.
[43] J A Stratton. *Electromagnetic Theory*. McGraw-Hill, New York, 1941.
[44] R Streich. 3d finite-difference frequency-domain modeling of controlled-source electromagnetic data: Direct solution and optimization for high accuracy. *Geophysics*, 74:F95, 2009.
[45] A H Stroud and D Secrest. *Gaussian quadrature formulas*. Prentice-Hall, 1966.
[46] A Tarantola. *Inverse Problem Theory*. Elsevier, 1987.
[47] J. Virieux, C. Flores-Luna, and D. Gilbert. Asymptotic theory for diffusive electromagnetic imaging. *Geophysical Journal International*, 119:857–868, 1994.
[48] J R Wait. Electromagnetic propagation in an idealized earth crust waveguide. *Radio Science*, 1:913–924, 1966.
[49] M Wheeler. An elliptic collocation-finite element method with interior penalties. *SIAM Journal on Numerical Analysis*, 15:152–161, 1978.
[50] P D Young and C S Cox. Electromagnetic active source sounding near the east pacific rise:. *Geophysical Research Letters*, 8:1043–1046, 1981.
[51] A Ziolkowski, B A Hobbs, and D Wright. Multitransient electromagnetic demonstration survey in france. *Geophysics*, 72:F197–F209, 2007.